ACS Biomaterials SCIENCE & ENGINEERING
Cite This: ACS Biomater. Sci. Eng. 2019, 5, 2482−2490
Article
pubs.acs.org/journal/abseba

In Vivo Human Cartilage Formation in Three-Dimensional Bioprinted Constructs with a Novel Bacterial Nanocellulose Bioink

Peter Apelgren,[†] Erdem Karabulut,[‡,§] Matteo Amoroso,[†] Athanasios Mantas,[‡] Héctor Martínez Ávila,[‡] Lars Kölby,[†] Tetsuo Kondo,[∥] Guillermo Toriz,[⊥] and Paul Gatenholm*[,‡,§]

[†]Sahlgrenska Academy, Institute of Clinical Sciences, Department of Plastic Surgery, Sahlgrenska University Hospital, Gothenburg University, Gothenburg 41685, Sweden

[‡]3D Bioprinting Center, BBV at Biotech Center, Gothenburg 41346, Sweden

[§]Wallenberg Wood Science Center, Department of Chemistry and Chemical Engineering, Chalmers University of Technology, Gothenburg 41296, Sweden

[∥]Biomacromolecular Materials Lab, and Biomaterial Design Lab, Graduate School of Bioresource and Bioenvironmental Sciences, Kyushu University, 6-10-1, Hakozaki, Higashi-ku, Fukuoka 812-8581, Japan

[⊥]Wood, Cellulose and Paper Research, University of Guadalajara, Guadalajara 44100, Mexico

Supporting Information

ABSTRACT: Bacterial nanocellulose (BNC) is a 3D network of nanofibrils exhibiting excellent biocompatibility. Here, we present the aqueous counter collision (ACC) method of BNC disassembly to create bioink with suitable properties for cartilage-specific 3D-bioprinting. BNC was disentangled by ACC, and fibril characteristics were analyzed. Bioink printing fidelity and shear-thinning properties were evaluated. Cell-laden bioprinted grid constructs ($5 \times 5 \times 1$ mm^3) containing human nasal chondrocytes (10 M mL^{-1}) were implanted in nude mice and explanted after 30 and 60 days. Both ACC and hydrolysis resulted in significantly reduced fiber lengths, with ACC resulting in longer fibrils and fewer negative charges relative to hydrolysis. Moreover, ACC-BNC bioink showed outstanding printability, postprinting mechanical stability, and structural integrity. In vivo, cell-laden structures were rapidly integrated, maintained structural integrity, and showed chondrocyte proliferation, with 32.8 ± 13.8 cells per mm^2 observed after 30 days and 85.6 ± 30.0 cells per mm^2 at day 60 (p = 0.002). Furthermore, a full-thickness skin graft was attached and integrated completely on top of the 3D-bioprinted construct. The novel ACC disentanglement technique makes BNC biomaterial highly suitable for 3D-bioprinting and clinical translation, suggesting cell-laden 3D-bioprinted ACC-BNC as a promising solution for cartilage repair.

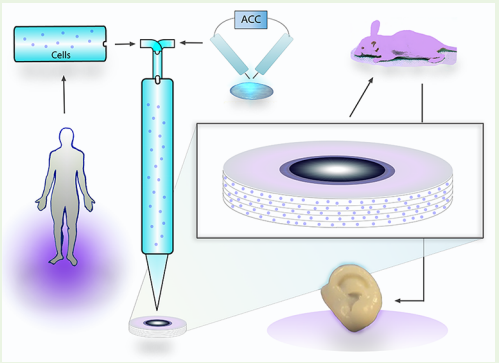

KEYWORDS: *3D-bioprinting, bacterial nanocellulose, aqueous counter collision, bioinks, neocartilage formation*

1. INTRODUCTION

Deficient or absent cartilaginous tissues and organs pose a significant challenge in reconstructive plastic surgery. Existing surgical methods involving autologous transplantations of cartilage are technically demanding for the plastic surgeon and strenuous for the patients.[1] 3D-bioprinting is an emerging technology where living cells can be spatially arranged by depositing cells and scaffolding biomaterial in any shape using a 3D-bioprinter. Chondrocytes and cartilaginous tissue are becoming a well-studied field in the 3D-bioprinting scientific community, with several reports show promising results.[2−5] However, challenges remain before an introduction of 3D-bioprinting of cartilage to the clinic. First, the scarcity of autologous progenitor cells (i.e., chondrocytes) from which chondrogenesis emanates needs to be addressed. One promising way to overcome this issue is to take advantage of the subsidiary proliferative effects of stem cells.[6] The beneficial presence of stem cells has been shown in several studies, with their boosting capability exerted through paracrine signaling.[7−9] Second, vascularization issues need to be resolved in order to enable reconstruction of larger, more complex composite structures. The diffusion of oxygen and nutrients is limited to ∼200 μm, and thicker structures require vascularization to survive and ensure sufficient neoangiogenesis.[10] Some studies utilized porous materials to reduce the diffusion distance,[11,12] whereas others addressed vascularization by introducing endothelial cells and prefabricated microscopic tubes to guide angiogenesis more efficiently.[13,14] A review by Rouwkema and Khademhosseini provides a comprehensive overview addressing these issues.[15] Third, long-term preclinical results need to be evaluated with regard to plausible ossification,[16−18] and neoplastic transformation,[19] as

Received: February 1, 2019
Accepted: March 21, 2019
Published: March 29, 2019

DOI: 10.1021/acsbiomaterials.9b00157
ACS Biomater. Sci. Eng. 2019, 5, 2482−2490

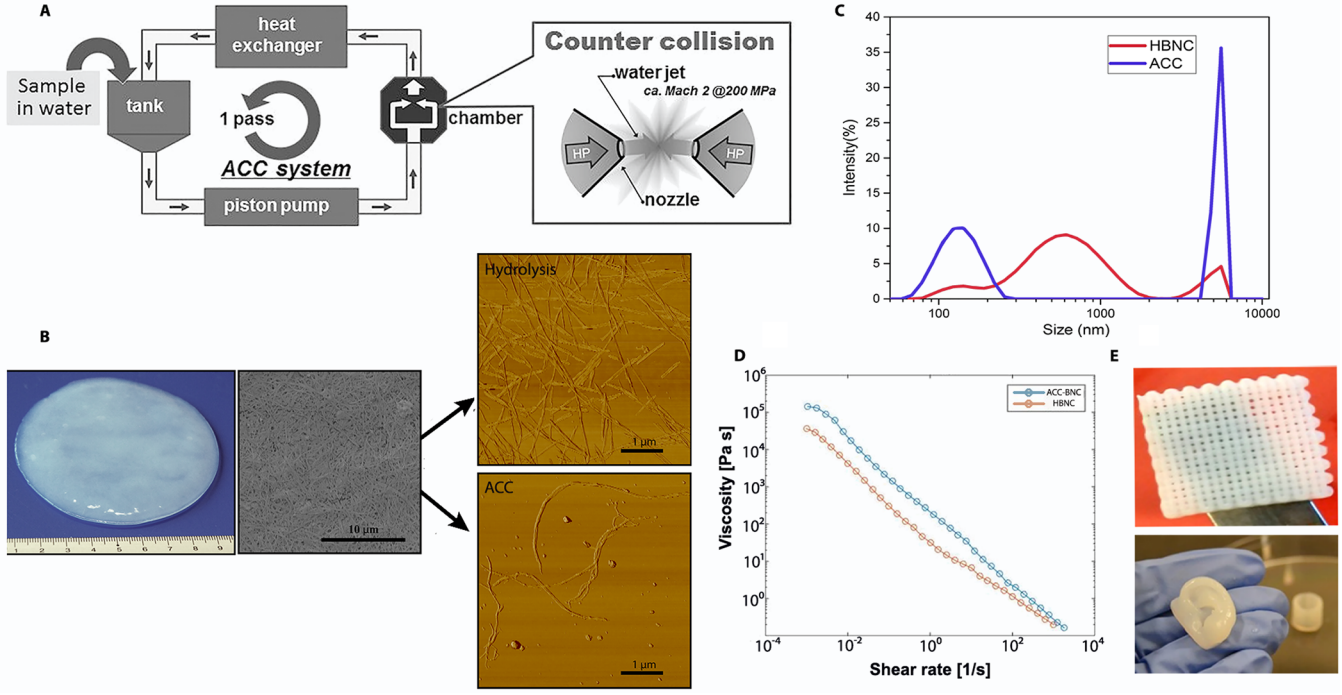

Figure 1. (A) ACC disassembly. Schematic representation of the ACC system using impinging dual aqueous-suspension jets. (B) Disassembly methods. After a 7 day cultivation, the BNC pellicle is mechanically stable, with its structural integrity due to the complex 3D network resulting from the bacterial bioassembly process. SEM analysis shows the highly entangled nanofibrillar network (scale bar = 10 μm). AFM after hydrolysis (top) and after ACC (bottom) disassembly (scale bars = 1 μm). (C) DLS analysis. The hydrodynamic size of hydrolyzed BNC (red) and ACC-treated BNC (blue). Longer fibrils are present in the ACC-BNC (logarithmic x-bar). (D) Rheology. Rheologic features of the shear-thinning behavior of the disassembled BNC hydrogels. Hydrolyzed BNC (red) and ACC-BNC (blue). The rheologic features were similar, but ACC-BNC needed only 2.5 wt % dry content as compared to 5 wt % required by hydrolyzed BNC. (E) Very good printing fidelity and resolution were exemplified by a bioprinted grid structure, and both bioinks were successfully used to bioprint an auricle and a self-supporting tube.

well as the preservation of coveted biomechanical features (e.g., elasticity, shape fidelity, and tissue integration).

In addition to these biological factors, the 3D-bioprinting technique needs to be adapted and improved biomechanically, particularly concerning the scaffolding biomaterial (i.e., bioink). 3D-bioprinting technology allows for micrometric precision of the architecture in the scaffolds and also provides a cell-friendly environment that is far more advantageous than other scaffold-producing methods, which struggle to control the 3D morphology, as well as the cell distribution, within the constructs.[20−27] Bioinks mimicking the biological and physical properties of extracellular matrix (ECM) are necessary for providing a cell-friendly environment. From a biological aspect, an ideal bioink must incorporate cells and other bioactive factors homogeneously and must not contain immunogenic and toxic byproducts of degradation. The printed constructs should have a good porosity for diffusion of oxygen, nutrients, and metabolites; can be processed under mild cell-friendly conditions; and should produce little to no irritation. So far, a range of natural polymers have been implemented and 3D-bioprinted especially for tissue regeneration. However, only a few of them have received a common interest due to printability issues and lack of complexity of natural extracellular matrix (ECM) and thus are unable to reconstitute the intrinsic cellular morphologies and functions.

A 3D-bioprinter can distribute several different types of cells with high spatial resolution, enabling the replication of the microarchitecture and complexity of human tissues and organs.[28] However, cell suspensions have low viscosity, making it impossible for the cells to remain in their predetermined positions. One way to overcome this is to combine human cells with a supporting biomaterial in the liquid phase (i.e., bioink). Hydrogels are suitable materials for bioinks used in 3D-bioprinting because of their high water content, which is a crucial environmental factor for cell survival.[29] A new generation of bioinks based on nanocellulose fibrils was recently introduced.[30] Nanocellulose fibrils biosynthesized by plants enable high printing fidelity, retained porosity, and, when combined with alginate, have been successfully evaluated for 3D-bioprinting of cartilage and adipose tissue.[8,30−33] In addition to biocompatibility, the bioink also needs to be printable with high resolution and exhibit good rheological properties and printability.

Bacteria-produced nanocellulose (BNC) is a nanostructured biomaterial of high purity and comprising strong nanofibrills ~30 nm in diameter and with lengths of several microns. BNC is produced by the Gram-negative bacteria *Gluconacetobacter xylinus*, and the 3D network of BNC possesses significant water-retention capacity (99 wt %).[34] Furthermore, BNC shows remarkable biocompatibility and tissue-integration capability due to its highly hydrated fibrils and their morphological similarity to components in the native extracellular matrix.[25,26,35−40] BNC is thoroughly biologically evaluated, Food and Drug Administration (FDA) approved for several applications, and, thus, readily transposable to human clinical use.[41,42] These characteristics enabled the introduction of BNC-constructed materials into the clinic for applications that include wound and burn dressings, such as Bioprocess (Fibrocel Produtos Bioetecnologicos, Curitiba, PR Brazil), XCell (Xylos Corporation, Langhorn, PA, USA), Dermafill

DOI: 10.1021/acsbiomaterials.9b00157
ACS Biomater. Sci. Eng. 2019, 5, 2482−2490

(Cellulose Solutions, Bainbridge, GA, USA), surgical meshes [e.g., Securian (Xylos Corporation, USA)], and dura mater substitutes [e.g., SyntheCel (DePuy Synthes Biomaterials, West Chester, PA, USA)]. The biotechnological production of BNC permits control of the network structure, as well as the 3D shaping and surface design of BNC implants. Consequently, BNC has also been fabricated with desired shapes and architectures for a variety of biomedical applications, including artificial blood vessels[20,21,23,24] and meniscus and auricular cartilage.[22,25] Additionally, BNC has been used to support osteoblasts, chondrocytes, fibroblasts, and stem cells.[27]

Among the most important material requirements for an ideal bioink are rheological properties, particularly shear-thinning properties. Biopolymers, such as collagen, alginate, hyaluronate, and chitosan, have been successfully evaluated as bioinks for printing human tissues, such as skin and cartilage.[43−48] However, the viscoelastic properties of these biopolymers have limitations when used as bioinks. The low viscosity at high shear rates, which corresponds to the flow conditions in the printing nozzle, is advantageous for high printing speed, but the stress-relaxation characteristics and the not sufficiently high viscosity at zero shear rates make it difficult to print these biopolymers with line widths <400 μm.[49] To mimic the microarchitecture of native organs and tissues, 3D-bioprinting requires much higher fidelity. Furthermore, postprinting, the bioink needs to be cross-linked in order to provide a mechanically stable construct. Cells encapsulated in such cross-linked constructs will not survive because of the diffusion limit of oxygen and nutrients. Therefore, the porosity of the constructs is also of major importance.

3D-bioprinting technology can be swiftly translated to the clinic when Food and Drug Administration-compliant biomaterials are used. Additionally, BNC biosynthesis can be performed in Good Manufacturing Practice facilities, including a meticulous purification process which yields a biomaterial with very low levels of endotoxins.[25] However, the biggest challenge with BNC use in 3D-bioprinting is the disentanglement of the extremely intricate BNC fibril network formed during biosynthesis, which is impervious to current defibrillation methods utilized to prepare plant-derived nanocellulose.[50] Without proper disentanglement, the fibrils flock and clog the nozzle of the bioprinter. Therefore, this issue has impeded the use of BNC as bioink.

Recently, a novel method for disintegrating hierarchically organized biobased materials into nanosized fibrils using the collision energy of dual water jets was invented by Kondo et al.[51−58] This technique, termed aqueous counter collision (ACC), successfully dissociates weaker intermolecular interactions, such as those joined by van der Waals forces in biobased materials, without any chemical modification. In the ACC system, an aqueous suspension containing microsized samples of the biomaterial is exposed to the water jets (Figure 1A), and as the water collides with the biomaterial, the water molecules transfer their kinetic energy, resulting in disintegration and fibril disentanglement. When ACC is applied to a bacterial cellulose pellicle, it disassembled into single cellulose nanofibrils. As shown with transmission electron microscopy (TEM) analysis by Kose et al.,[55] the length and width of the ACC-BNC fibrils decrease along with increasing ACC passes. Furthermore, they also demonstrated evidence of changing surface characteristics imposed by the ACC treatment. BNC secreted by *G. xylinus* comprises two crystalline phases: cellulose Iα and Iß (at a 65%:35% ratio).[59,60] In subsequent studies of the ACC technique, Kondo et al.[53] showed that the ratio of cellulose Iα relative to that in total crystal phases in native BNC decreases along with the number of passes, whereas the cellulose Iβ phase increases.

The present study compares two fibril disassembly methods, hydrolysis or ACC disintegration, for the creation of a 3D-bioprinter-compatible BNC bioink. Here, we describe the entire sequence from the biosynthesis of bacterial cellulose, purification, disassembly, and bioink preparation to verification of BNC adequacy as a bioink for 3D-bioprinting of human chondrocytes in vivo.

2. EXPERIMENTAL SECTION

2.1. BNC Biosynthesis. Bacterial growth media[61] (50 mL) in Petri dishes (9 cm in diameter) were inoculated with precultured *G. xylinus* subspecies *sucrofermentas* (BRP2001; 700178; LGC Promochem, Borås, Sweden) and placed in an incubator at 30 °C for 7 days. The obtained BNC pellicle was purified in an in-house-built perfusion system as described previously.[25] Briefly, the BNC was perfused with 0.5 M sodium hydroxide (NaOH) at a flow rate of 5000 L h^{-1} and a pressure of 50 kPa for 28 days. The alkaline solution was replaced every second to third day and was then removed from the BNC by perfusing it with deionized (DI) water until the pH of the drained water was ∼7. The DI water was replaced every day for 7 days, after which the BNC was washed with Milli-Q water (Merck Millipore, Billerica, MA, USA) to further remove the alkaline solution and neutralize the pH. The Milli-Q water was replaced twice daily for 7 days and rinsed with endotoxin-free water (HyClone cell-culture-grade water; Thermo Fisher Scientific, Waltham, MA, USA), followed by steam sterilization (100 kPa at 121 °C for 20 min; Varioklav Steam Sterilizer 135T; Thermo Fisher Scientific) and then disassembly.

2.2. BNC Disassembly by Hydrolysis. Hydrolysis was performed by treating 100 g of BNC (1 g cellulose) with 19 wt % sulfuric acid at 60 °C for 24 and 48 h, after which the reaction system was cooled and neutralized with 1 M NaOH. The sample was then washed thoroughly with DI water and centrifuged five times for 15 min at 4000 rpm. The BNC was then resuspended in 300 mL of endotoxin-free water (HyClone cell-culture-grade water; Thermo Fisher Scientific) and homogenized at 20 000 rpm for 10 min (ULTRA-TURRAX; IKA, Staufen, Germany). The obtained colloidal dispersion was then centrifuged five times for 15 min at 4000 rpm. The dispersion was further concentrated to 4 wt % by means of ultrafiltration using a Waters ultrafiltration unit (Waters Corporation, Milford, MA, USA) and a polytetrafluoroethylene membrane with a 1 kDa molecular weight cutoff.

2.3. BNC Disassembly with ACC. Mechanical homogenization of the BNC pellicles was achieved by cutting them into small pieces, disintegrating them in a high-intensity mixer (0.4 wt % concentration at 20 000 rpm for 5 min; ULTRA-TURRAX; IKA), and then submitting the BNC dispersion to the ACC procedure (ACC system; Sugino Machine, Toyama, Japan) at 200 MPa of ejecting pressure in a cycle of 30 rounds. The ACC dispersion was concentrated to 2.5 wt % by centrifugation (JOUAN CR 3i multifunction; Thermo Fisher Scientific), and the supernatant excess was removed. A complete description of the ACC method can be found in Kondo et al.[54]

2.4. SEM and AFM. SEM was used to provide an explicative overview of the intricate fibril network in the BNC before disassembly (the SEM method is described in Supporting Information S1). AFM was used to measure the fiber dimensions in both ACC-BNC and hydrolyzed BNC (the AFM method is described in Supporting Information S2).

2.5. DLS. The average hydrodynamic size and zeta (ζ-potential, i.e., the average charge of the fibrils) of the hydrolyzed and ACC-treated BNC were measured using DLS (Nano ZS-ZEN3600; Malvern Instruments, Malvern, UK).

DOI: 10.1021/acsbiomaterials.9b00157
ACS Biomater. Sci. Eng. 2019, 5, 2482−2490

2.6. Rheology. Rheological properties were evaluated in both ACC-BNC and hydrolyzed BNC. These methods are described in Supporting Information S3.

2.7. Cells. hNCs were harvested from a male donor undergoing septum rhinoplasty at the Department of Otorhinolaryngology of Ulm University Medical Centre (Ulm, Germany). The harvesting was approved by the Ethical Advisory Board at Ulm University (Dnr 152/08). The chondrocytes were cultured in Dulbecco's modified Eagle medium/F-12 (Life Technologies, Waltham, MA, USA) supplemented with 10% fetal bovine serum (HyClone; GE Healthcare, South Logan, UT, USA) and 1% penicillin/streptomycin (HyClone; GE Healthcare) for 6 days before printing.

Preceding the mixing procedure with the ACC-BNC, the cells were trypsinized, centrifuged, and counted using the trypan blue dye-exclusion method.[65] The mixing procedure of the bioink and cells was performed with a cell mixer (CELLINK AB, Gothenburg, Sweden) at an 11:1 ratio. The final bioink cell density was 10 M cells mL^{-1}.

2.8. Bioink Preparation. For preparation of the bioinks, hydrolyzed BNC (5 wt % dry content) or ACC-BNC (2.5 wt % dry content) was mixed with D-mannitol (Sigma-Aldrich, St. Louis, MO, USA) to reach 4.6 wt % mannitol in the aqueous phase in order to retain the osmolarity.[62] The dispersion was then sterilized by an electron beam at 25 Gy for 5 min (Herotron E-Beam Service, Bitterfeld-Wolfen, Germany).

Sterile alginate (SLG100 Mw: 150−250 kDa; FMC Biopolymers, Oslo, Norway) containing >60% of α-1-guluronic acid and diluted to a concentration of 2.5% (w/v) in a 4.6% (w/v) aqueous solution of D-mannitol was used to prepare the bioinks by mixing at an 80:20 BNC/alginate ratio.

2.9. 3D-Bioprinting. 3D-bioprinting was performed using two different printers. For explicative shapes (an auricle, a hollow tube, and a high-resolution grid), a Discovery printer (RegenHu, Villaz-St-Pierre, Switzerland) was used (this method is described in Supporting Information S4). For in vivo analyses, an INKREDIBLE printer (CELLINK AB) was used (this method is described in Supporting Information S5).

2.10. Animals. Female, nude Balb/C mice (n = 26; 8-weeks old; Scanbur, Karlslunde, Denmark) were used for the animal studies. Animals were kept on a sawdust floor in macrolon cages at room temperature (20 °C) and illumination on a 12 h/12 h light/dark cycle. Food and water were ad libitum, and the well-being of the animals was assessed daily by animal keepers and, if needed, a veterinarian. Animal experiments were approved by the Ethics Committee for experimental animals at the University of Gothenburg (Dnr 119-2015).

2.11. Experimental Design. The animals were divided into two groups: those in A (n = 12) carried the cell-laden constructs, and those in B (n = 12) carried the cell-free constructs. The constructs were surgically implanted in subcutaneous pockets on the backs of the mice. Intraperitoneal injection of a mixture of ketamine (50 mg/mL) and medetomidine (1 mg/mL) at a 1.5:1 ratio induced general anesthesia. Each animal received 0.04 mL of anesthetic solution per 20 g body weight. The pockets were closed with Vicryl Rapid (Ethicon, Sommerville, NJ, USA).

After 30 and 60 days, respectively, the mice were euthanized and the constructs retrieved, fixated in 4% buffered formaldehyde supplemented with 20 mM $CaCl_2$ overnight at 4 °C, and embedded in paraffin.

Additionally, and consistent with a clinical point of view, we added a third group with only two animals. One of these two received an ACC-BNC construct with hNCs similar to those in group A, but was again anesthetized on day 45. The other mouse served as a full-thickness skin-graft donor. The skin graft was sutured onto the BNC-hNC construct with microsutures (Prolene 8−0; Ethicon), and the transplanted and native skin was also sutured edge-to-edge. On day 60, the construct and skin were excised and submitted to the same preparations as described above for groups A and B.

2.12. Morphological Analysis. For morphological analysis and analysis of glycosaminoglycan (GAG) production, one core section (5 μm) from every explanted construct was chosen. Deparaffinized sections were stained with Alcian Blue and van Gieson and scanned using a Nikon Eclipse 90i epi-fluorescence microscope equipped with a Nikon DS-Fi2 color head camera and NIS-Elements software (vD4.10.02; Nikon Instruments, Melville, NY, USA). The images were imported into PhotoShop (Adobe Systems, San Jose, CA, USA), and the area of the sections was determined.

All GAG-positive cells, defined as a cell nucleus surrounded by blue-stained GAGs in the extracellular matrix, in each section were manually counted, and the regions occupied with GAG-positive cells were encircled. The number of GAG-positive cells was presented as the number of cells ± standard deviation (SD) per mm^2. The GAG-positive cell-cluster areas were related to the area of the section. Additional information about the histological sections is provided in Figure S1. Immunohistochemical and FISH analyses are described in detail in Supporting Information S6 and S7.

2.13. Statistical Analysis. An independent Student's t test was used to compare the mean number of cells per mm^2 and the mean percentage of the section area occupied by GAG-positive cell clusters (30 vs 60 days). All statistical calculations were performed using SPSS (v22.0; IBM SPSS, Armonk, NY, USA). A $p < 0.05$ was considered statistically significant.

3. RESULTS

3.1. BNC Disassembly. *3.1.1. Scanning Electron Microscopy (SEM) and Atomic Force Microscopy (AFM) Analyses.* Both methods for disentanglement of the BNC resulted in significant reductions in fiber length and cross-section diameter. AFM height images revealed that the BNC fibrils were well-separated from each other after both hydrolysis and ACC treatment. The average fibril diameter and length was 16 ± 0.07 nm and 2 ± 0.4 μm, respectively, and the root-mean-square surface roughness was 30 nm (Figure 1B).

3.1.2. Dynamic Light Scattering (DLS) and ζ-Potential. DLS analysis of the distributions of the fibril hydrodynamic sizes of the ACC-treated BNC showed a bimodal distribution, with ∼50% of the fibers ranging from 70 to 200 nm and the rest at between 5 and 6 μm. By contrast, in hydrolyzed BNC, only ∼12% of the fibers ranged from 80 to 200 nm, whereas a substantial portion (75%) ranged from 250 to 1900 nm and the rest (12%) from 5 to 6 μm. The average fibril length of hydrolyzed BNC was 1.25 ± 0.97 μm, whereas ACC-treated BNC showed two distinct fibril sizes (denoting the multimodal distribution of the fibrils), with one in the range of >3 μm, whereas BNC particles were in the range of 120 nm (Figure 1C).

The hydrodynamic size of the hydrolyzed BNC showed a trimodal pattern centered at 120 nm, 615 nm, and 5.6 μm. These patterns were consistent with AFM images and measurements. Furthermore, the ζ-potential of the hydrolyzed BNC was considerably more negatively charged (−27.9 mV) as compared with ACC-BNC (−11.3 mV).

3.1.3. Rheology. Both materials showed excellent shear-thinning behavior and a wide biofabrication window (Figure 1D). Due to the longer fibrils and despite much lower solid content, the ACC-treated BNC had a higher viscosity as compared with that of the hydrolyzed BNC. The printabilities of both bioinks were similar.

ACC-BNC was selected for in vivo evaluation due to its higher viscosity at lower nanocellulose concentration. Human nasal chondrocyte-laden constructs were 3D-bioprinted and implanted in naked mice. See section 2.11 for details.

3.2. Chondrogenesis in Vivo. Of the 26 animals, 25 survived and could be sacrificed as planned. The one that did not survive was found dead in the cage on the first

DOI: 10.1021/acsbiomaterials.9b00157
ACS Biomater. Sci. Eng. 2019, 5, 2482−2490

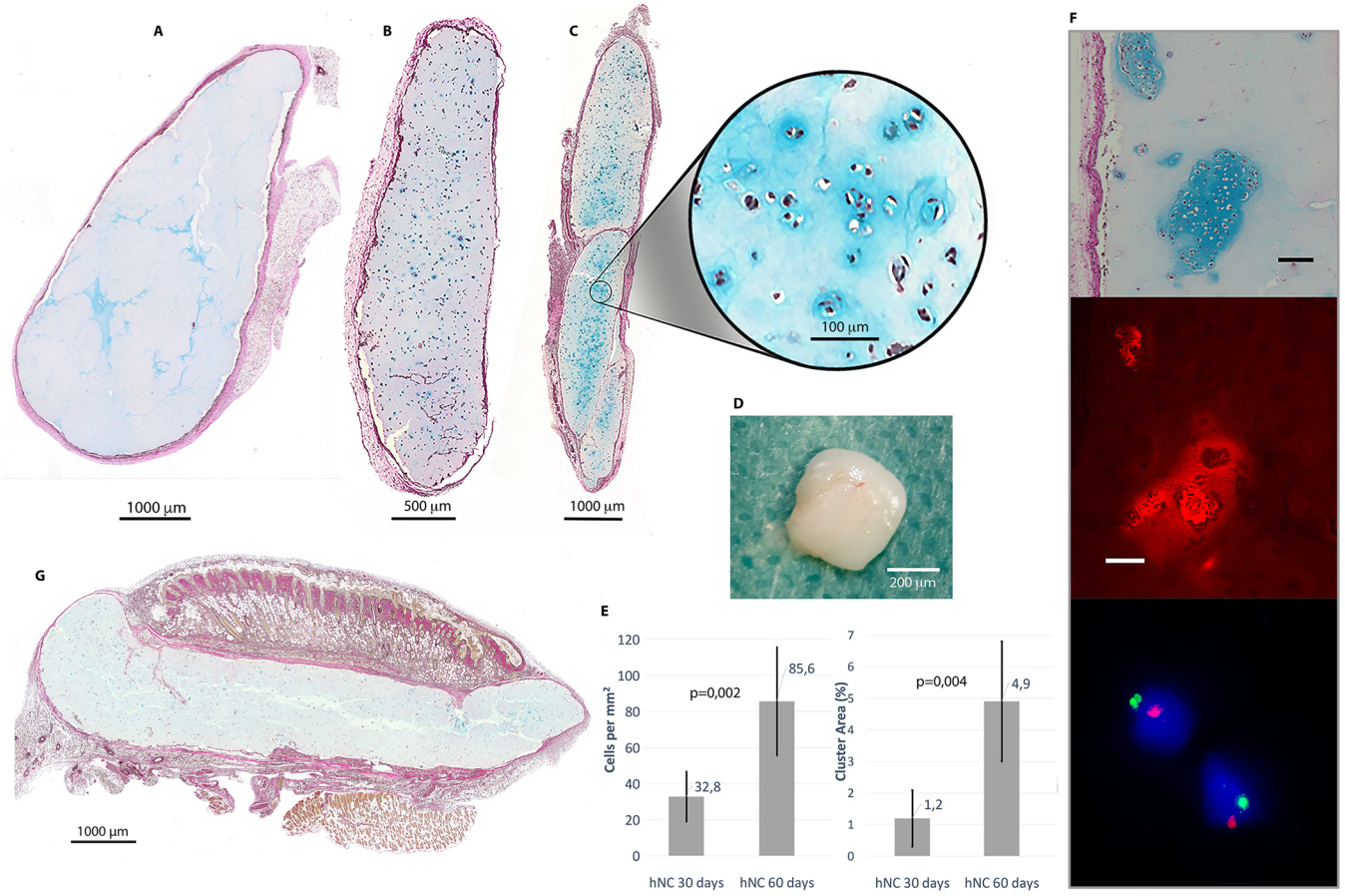

Figure 2. Cartilage formation. No GAG-positive cells were detected in the cell-free controls (A). A significant proliferative effect was observed between days 30 (B) and 60 (C). Magnification shows the cluster formations. Scale bars = 1000, 500, and 1000 μm, respectively. (D) Explanted construct. Macroscopic appearance of ACC-treated and 3D-bioprinted BNC constructs at 60 days after subcutaneous implantation in a nude mouse. A thin fibrous film encapsulates the construct, and angiogenesis can be observed macroscopically. The construct had retained its 3D shape and was easy to handle surgically. (E) Chondrocyte proliferation. Bar charts showing cells/mm^2 (left) and cluster area (right). (F) Immunohistological and FISH analyses. The Alcian Blue staining of glycoseaminoglycans (top) corresponding well to the Collagen 2 depositions (bright red, middle). FISH analysis (bottom) confirmed that the chondrocytes were of human origin, as well as derived from the male chondrocytes. Scale bars = 100 μm. (G) Skin transplantation. Histological section of the skin graft on top of the ACC-BNC construct at 15 days after transplantation. Alcian Blue and van Gieson staining show GAG-producing chondrocytes. The skin transplant is fully integrated, and there are no signs of necrosis or adverse tissue reactions. Scale bar = 1000 μm.

postoperative day and belonged to the control group for the study planned for day 60.

Macroscopically, the constructs were well-integrated and had retained their 3D shape. The explanted 3D-bioprinted constructs were white, shiny, and elastic and exhibited excellent mechanical handling properties (Figures 1E and 2D).

Cartilage formation was observed in the human nasal chondrocyte (hNC) group, as reflected by both a gradual increase in the number of chondrocytes and a gradually increased deposition of glycosaminoglycans from day 30 to day 60. There was also evidence of chondrocyte proliferation based on the formation of clusters of GAG-positive cells. The clusters were generally small, containing only two to five cells, but we also observed larger clusters of up to 40 cells.

Group A (ACC-BNC with hNC) showed an abundance of GAG-positive cells (Figure 2B,C), and at day 30, there were 32.8 ± 13.8 (mean ± SD) cells per mm^2. During the time course of the experiment, the number of cells increased significantly, and at day 60, there were 85.6 ± 30.0 cells per mm^2 (p = 0.002). Additionally, the percentage of the area occupied by GAG-positive cells increased significantly from 1.2 ± 0.9% to 4.9 ± 1.9% (p = 0.004) at days 30 and 60, respectively (Figure 2E). In group B (cell-free constructs), no GAG-positive cells were found (histological images in Figure 2A and in Figure S2).

Immunohistochemical analysis revealed production of human collagen type 2 in the same areas as that indicated by the blue-stained glycosaminoglycans. Fluorescence in situ hybridization (FISH) analysis confirmed that the GAG-positive cells in the 3D-bioprinted constructs were mainly of human origin and stained positive for both human X and Y chromosomes, indicating that they were of male origin (i.e., derived from chondrocytes) (Figure 2F). The immunohistochemical and FISH methods are described in Supporting Information S6 and S7, respectively.

3.3. Skin Transplantation. The skin transplant had integrated completely at 15 days after transplantation both macroscopically and histologically (Figure 2G), with no adverse tissue reactions, such as necrosis, observed. Additionally, viable and GAG-producing chondrocytes were observed in the ACC-BNC construct. Macroscopic images of the transplanted skin are provided in Figure S3.

DOI: 10.1021/acsbiomaterials.9b00157
ACS Biomater. Sci. Eng. 2019, 5, 2482−2490

4. DISCUSSION

The excellent biocompatibility, rheological properties, printability, tissue integration, and subsidizing features for proliferation observed in vivo show that BNC disentangled by the novel technique ACC represents a promising biomaterial for bioprinting of human cartilage. This study assessed the properties crucial for the use of BNC in chondrogenesis with 3D-bioprinting technology. Additionally, our in vivo experimental methodology was established to mimic a real clinical situation.

Our results showed that the ACC method can be used to create a printable hydrogel that provides a highly favorable milieu for human cells. The fibril morphology of the bioink played a decisive role in cell behavior, likely due to differences in surface crystallinity. The ACC-treated BNC retained most of the crystallinity, thereby allowing the Iβ allomorph to develop at the surface.

According to previous surface analysis conducted by Kondo et al.,[54,56] ACC-induced pulverization of BNC led to unfolding and exposure of internal surfaces, thereby increasing the total surface area.[57] The high adsorptivity found in the ACC-BNC is most likely explained by the increased specific surface areas. Additionally, the surface exposure of a larger portion of the Iβ allomorph in the ACC-BNC is expected to exhibit increased resistance against chemical reagents and less susceptibility to enzymatic degradation as compared with the initial microbial cellulose pellicle.

The transformation from crystallinity phase Iα to Iβ occurred on the nanofiber surface, suggesting that the shear-stress force conveyed by the collision energy of water at high pressure in the ACC procedure caused rearrangement of cellulose-molecule crystallinity. A previous study from Yamamoto et al. reported that the Iβ phase was thermodynamically more stable than the Iα phase.[63] A subsequent study from the same group also proposed that BNC secreted by *G. xylinus* comprises a core of Iβ-rich domains surrounded by a surface layer of cellulose Iα-rich domains.[60] According to this theory, a larger proportion of the more stable phase-Iβ-enriched crystalline core is unfolded and exposed in ACC-treated BNC, whereas the more fragile Iα-phase domains are covered and, thus, protected by an outer surface of the more resilient Iβ phase. The resulting advantageous features of ACC-BNC are likely partially explained by this crystalline transformation. The size distribution of the fibrils, with longer fibrils observed in ACC-treated BNC, can also have a positive effect on cell behavior. The lower negative-charge density (i.e., ζ-potential) of the ACC-BNC fibrils might also advantageously affect cell interactions.

Additionally, ACC-BNC showed a suitable rheological profile, which is of central importance in the printability of a bioink. The high water-binding capacity of these long fibrils results in a bioink that needs only half the dry weight ACC-BNC content as compared with hydrolyzed BNC, resulting in a bioprinted structure containing less foreign material and making it more attractive for use in clinical situations. Furthermore, the postprinting shape fidelity of the constructs was good and withstood degradation and decomposition in vivo, with the explanted constructs largely unaffected after 2 months. Increased stiffness over time of the implanted 3D-bioprinted BNC constructs containing chondrocytes as opposed to cell-free constructs has been reported previously.[8] The mechanism associated with this favorable development has not yet been elucidated. In the present study, increased chondrocyte number over time was accompanied by increases in GAG-positive areas. The 3D-bioprinted cartilage was also positive for collagen type 2, as expected in hyaline cartilage. Therefore, it is plausible that the adequate matrix components produced by the thriving chondrocytes are responsible for the increased stiffness over time.

It is possible that chondrocyte proliferation will continue, and that the number of matrix molecules will increase further, eventually resulting in dense cartilaginous tissue. However, this requires further testing in future studies, which also need to evaluate the quality of the bioprinted cartilage in terms of mechanical properties.

As a proof-of-concept to one crucial part of the future clinical applicability, a skin graft was transplanted on top of the 3D-bioprinted BNC construct. The clinical counterpart could be, for example, auricle reconstruction where the 3D-bioprinted cartilaginous ear-shaped structures have to be covered with skin, either with a skin graft, or with a flap. In this study, no dehiscence or necrosis could be seen in the histological analysis. This indicates that the 3D-bioprinted BNC construct was able to provide the graft with sufficient oxygen and nutrients before the neoangiogenic process had been established.

For example, one clinical counterpart of the technology described in the present study is auricular reconstructions. The patient's contralateral auricle is first scanned with MRI or a 3D camera to generate the blueprint for the printer. Autologous cells are harvested and mixed with the bioink, and the cell-containing scaffold is printed by the 3D-bioprinter. The new auricular construct is then implanted subcutaneously on the patient's forearm. Several weeks later, the patient is scheduled for surgery, where the construct and the concomitant vessels are detached and transposed to the right place. The transplant is attached to temporal vessels via a microsurgical anastomosis technique and, finally, covered with a split-thickness graft or a local flap. Another clinical approach regarding nose reconstruction using 3D-bioprinting technology has recently been presented by Yi et al.[64]

Studies supporting FDA approval of BNC for use in humans established an indisputable safety profile for some applications of BNC,[65,66] and the present study contributes to BNC implementation in 3D-bioprinting technology. However, further studies are required prior to clinical application. For example, the inevitable degradation and subsequent loss of support from the cellulose scaffolds will need to be assessed over a longer period of time. Furthermore, potential deviation to an endochondral ossification lineage, as well as conceivable tumorigenesis, needs to be assessed in detail.

Moreover, the ACC-BNC bioinks need to be tested in immune-competent animal models, such as mammalian models of higher complexity (e.g., pigs), to evaluate the influence of the unavoidable inflammatory response to all types of transplantation of nonautologous material. Pigs utilize the same skin-healing process as humans, making them a suitable model. It is also worth noting that, in addition to immunological deficiencies in nude mice, other differences might also play a significant role in the overall healing process, such as the presence of an additional muscle layer (panniculus carnosus) in rodent skin anatomy.

DOI: 10.1021/acsbiomaterials.9b00157
ACS Biomater. Sci. Eng. 2019, 5, 2482−2490

5. CONCLUSIONS

In this study, a novel method for disassembling BNC was evaluated, with the results indicating that ACC treatment is a useful method for rendering a printable material with sufficient postprinting mechanical stability, as well as other advantageous features, such as high water-retention capacity. Upon the introduction of human cells, we observed excellent chondrocyte-proliferation capacity and tissue integration in vivo at 60 days after implantation in nude mice. Our findings suggest that the novel ACC disentanglement technique renders BNC bioink highly suitable for 3D-bioprinting in reconstructive surgery.

■ ASSOCIATED CONTENT

Supporting Information

The Supporting Information is available free of charge on the ACS Publications website at DOI: 10.1021/acsbiomaterials.9b00157.

Additional details regarding SEM analysis, AFM analysis, rheology, injet method, and extrusion method, and figures showing additional results (PDF)

■ AUTHOR INFORMATION

Corresponding Author

*E-mail: paul.gatenholm@chalmers.se.

ORCID

Tetsuo Kondo: 0000-0003-4366-2955

Paul Gatenholm: 0000-0002-5107-0389

Author Contributions

The manuscript was written through contributions of all authors. All authors have given approval to the final version of the manuscript.

Funding

No relevant funding was received for this research.

Notes

The authors declare the following competing financial interest(s): H.M.A. declares corporate engagement with Cellink AB. The other authors have no conflicts of interest to declare.

■ ACKNOWLEDGMENTS

We gratefully acknowledge M.Sc. Inger Ögärd and M.Sc. Camilla Brantsing for their expertise in FISH and immunohistochemistry.

■ REFERENCES

(1) Lindahl, A. From gristle to chondrocyte transplantation: treatment of cartilage injuries. *Philos. Trans. R. Soc., B* **2015**, *370* (1680), 20140369.

(2) Firmin, F. State-of-the-art autogenous ear reconstruction in cases of microtia. *Adv. Otorhinolaryngol* **2010**, *68*, 25−52.

(3) Firmin, F.; Marchac, A. A novel algorithm for autologous ear reconstruction. *Semin Plast Surg* **2011**, *25* (4), 257−64.

(4) Osorno, G. Autogenous rib cartilage reconstruction of congenital ear defects: report of 110 cases with Brent's technique. *Plast Reconstr Surg* **1999**, *104* (7), 1951−62. discussion 1963-4.

(5) Zopf, D. A.; Iams, W.; Kim, J. C.; Baker, S. R.; Moyer, J. S. Full-thickness skin graft overlying a separately harvested auricular cartilage graft for nasal alar reconstruction. *JAMA Facial Plast Surg* **2013**, *15* (2), 131−4.

(6) Wu, L.; Leijten, J. C.; Georgi, N.; Post, J. N.; van Blitterswijk, C. A.; Karperien, M. Trophic effects of mesenchymal stem cells increase chondrocyte proliferation and matrix formation. *Tissue Eng., Part A* **2011**, *17* (9−10), 1425−36.

(7) Aung, A.; Gupta, G.; Majid, G.; Varghese, S. Osteoarthritic chondrocyte-secreted morphogens induce chondrogenic differentiation of human mesenchymal stem cells. *Arthritis Rheum.* **2011**, *63* (1), 148−58.

(8) Moller, T.; Amoroso, M.; Hagg, D.; Brantsing, C.; Rotter, N.; Apelgren, P.; Lindahl, A.; Kolby, L.; Gatenholm, P. In Vivo Chondrogenesis in 3D Bioprinted Human Cell-laden Hydrogel Constructs. *Plast Reconstr Surg Glob Open* **2017**, *5* (2), e1227.

(9) Wu, L.; Leijten, J.; van Blitterswijk, C. A.; Karperien, M. Fibroblast growth factor-1 is a mesenchymal stromal cell-secreted factor stimulating proliferation of osteoarthritic chondrocytes in co-culture. *Stem Cells Dev.* **2013**, *22* (17), 2356−67.

(10) Kang, H. W.; Lee, S. J.; Ko, I. K.; Kengla, C.; Yoo, J. J.; Atala, A. A 3D bioprinting system to produce human-scale tissue constructs with structural integrity. *Nat. Biotechnol.* **2016**, *34* (3), 312−9.

(11) Nava, M. M.; Draghi, L.; Giordano, C.; Pietrabissa, R. The effect of scaffold pore size in cartilage tissue engineering. *J. Appl. Biomater. Funct. Mater.* **2016**, *14* (3), e223.

(12) O'Brien, F. J.; Harley, B. A.; Waller, M. A.; Yannas, I. V.; Gibson, L. J.; Prendergast, P. J. The effect of pore size on permeability and cell attachment in collagen scaffolds for tissue engineering. *Technol. Health Care* **2007**, *15* (1), 3−17.

(13) Burghartz, M.; Gehrke, T.; Storck, K.; Staudenmaier, R.; Mandlik, V.; Schurr, C.; Hoang, N.; Hagen, R.; Kleinsasser, N. Vascularization of engineered cartilage constructs in a mouse model. *Cell Tissue Res.* **2015**, *359* (2), 479−487.

(14) Nakano, K.; Murata, K.; Omokawa, S.; Akahane, M.; Shimizu, T.; Kawamura, K.; Kawate, K.; Tanaka, Y. Promotion of Osteogenesis and Angiogenesis in Vascularized Tissue-Engineered Bone Using Osteogenic Matrix Cell Sheets. *Plast Reconstr Surg* **2016**, *137* (5), 1476−84.

(15) Rouwkema, J.; Khademhosseini, A. Vascularization and Angiogenesis in Tissue Engineering: Beyond Creating Static Networks. *Trends Biotechnol.* **2016**, *34* (9), 733−45.

(16) Bahney, C. S.; Hu, D. P.; Taylor, A. J.; Ferro, F.; Britz, H. M.; Hallgrimsson, B.; Johnstone, B.; Miclau, T.; Marcucio, R. S. Stem cell-derived endochondral cartilage stimulates bone healing by tissue transformation. *J. Bone Miner. Res.* **2014**, *29* (5), 1269−82.

(17) Farrell, E.; Both, S. K.; Odorfer, K. I.; Koevoet, W.; Kops, N.; O'Brien, F. J.; Baatenburg de Jong, R. J.; Verhaar, J. A.; Cuijpers, V.; Jansen, J.; Erben, R. G.; van Osch, G. J. In-vivo generation of bone via endochondral ossification by in-vitro chondrogenic priming of adult human and rat mesenchymal stem cells. *BMC Musculoskeletal Disord.* **2011**, *12*, 31.

(18) Scotti, C.; Tonnarelli, B.; Papadimitropoulos, A.; Scherberich, A.; Schaeren, S.; Schauerte, A.; Lopez-Rios, J.; Zeller, R.; Barbero, A.; Martin, I. Recapitulation of endochondral bone formation using human adult mesenchymal stem cells as a paradigm for developmental engineering. *Proc. Natl. Acad. Sci. U. S. A.* **2010**, *107* (16), 7251−6.

(19) Ridge, S. M.; Sullivan, F. J.; Glynn, S. A. Mesenchymal stem cells: key players in cancer progression. *Mol. Cancer* **2017**, *16* (1), 31.

(20) Backdahl, H.; Helenius, G.; Bodin, A.; Nannmark, U.; Johansson, B. R.; Risberg, B.; Gatenholm, P. Mechanical properties of bacterial cellulose and interactions with smooth muscle cells. *Biomaterials* **2006**, *27* (9), 2141−9.

(21) Bodin, A.; Backdahl, H.; Fink, H.; Gustafsson, L.; Risberg, B.; Gatenholm, P. Influence of cultivation conditions on mechanical and morphological properties of bacterial cellulose tubes. *Biotechnol. Bioeng.* **2007**, *97* (2), 425−34.

(22) Bodin, A.; Concaro, S.; Brittberg, M.; Gatenholm, P. Bacterial cellulose as a potential meniscus implant. *J. Tissue Eng. Regener. Med.* **2007**, *1* (5), 406−8.

(23) Klemm, D.; Schumann, D.; Udhardt, U.; Marsch, S. Bacterial synthesized cellulose - Artificial blood vessels for microsurgery. *Prog. Polym. Sci.* **2001**, *26* (9), 1561−1603.

(24) Malm, C. J.; Risberg, B.; Bodin, A.; Backdahl, H.; Johansson, B. R.; Gatenholm, P.; Jeppsson, A. Small calibre biosynthetic bacterial

DOI: 10.1021/acsbiomaterials.9b00157
ACS Biomater. Sci. Eng. 2019, 5, 2482−2490

cellulose blood vessels: 13-months patency in a sheep model. *Scand. Cardiovasc. J.* **2012**, *46* (1), 57−62.
(25) Martinez Avila, H.; Schwarz, S.; Feldmann, E. M.; Mantas, A.; von Bomhard, A.; Gatenholm, P.; Rotter, N. Biocompatibility evaluation of densified bacterial nanocellulose hydrogel as an implant material for auricular cartilage regeneration. *Appl. Microbiol. Biotechnol.* **2014**, *98* (17), 7423−35.
(26) Svensson, A.; Nicklasson, E.; Harrah, T.; Panilaitis, B.; Kaplan, D. L.; Brittberg, M.; Gatenholm, P. Bacterial cellulose as a potential scaffold for tissue engineering of cartilage. *Biomaterials* **2005**, *26* (4), 419−31.
(27) Zaborowska, M.; Bodin, A.; Backdahl, H.; Popp, J.; Goldstein, A.; Gatenholm, P. Microporous bacterial cellulose as a potential scaffold for bone regeneration. *Acta Biomater.* **2010**, *6* (7), 2540−7.
(28) Murphy, S. V.; Atala, A. 3D bioprinting of tissues and organs. *Nat. Biotechnol.* **2014**, *32* (8), 773−85.
(29) Malda, J.; Visser, J.; Melchels, F. P.; Jungst, T.; Hennink, W. E.; Dhert, W. J.; Groll, J.; Hutmacher, D. W. 25th anniversary article: Engineering hydrogels for biofabrication. *Adv. Mater.* **2013**, *25* (36), 5011−28.
(30) Markstedt, K.; Mantas, A.; Tournier, I.; Martinez Avila, H.; Hagg, D.; Gatenholm, P. 3D Bioprinting Human Chondrocytes with Nanocellulose-Alginate Bioink for Cartilage Tissue Engineering Applications. *Biomacromolecules* **2015**, *16* (5), 1489−96.
(31) MartInez Avila, H.; Schwarz, S.; Rotter, N.; Gatenholm, P. 3D bioprinting of human chondrocyte-laden nanocellulose hydrogels for patient-specific auricular cartilage regeneration. *Bioprinting* **2016**, *1*−*2*, 22−35.
(32) Nguyen, D.; Hagg, D. A.; Forsman, A.; Ekholm, J.; Nimkingratana, P.; Brantsing, C.; Kalogeropoulos, T.; Zaunz, S.; Concaro, S.; Brittberg, M.; Lindahl, A.; Gatenholm, P.; Enejder, A.; Simonsson, S. Cartilage Tissue Engineering by the 3D Bioprinting of iPS Cells in a Nanocellulose/Alginate Bioink. *Sci. Rep.* **2017**, *7* (1), 658.
(33) Nimeskern, L.; Martinez Avila, H.; Sundberg, J.; Gatenholm, P.; Muller, R.; Stok, K. S. Mechanical evaluation of bacterial nanocellulose as an implant material for ear cartilage replacement. *J. Mech Behav Biomed Mater.* **2013**, *22*, 12−21.
(34) Gatenholm, P.; Klemm, D. Bacterial cellulose as a renewable material for biomedical applications. *MRS Bull.* **2010**, *35* (3), 208−213.
(35) Ahrem, H.; Pretzel, D.; Endres, M.; Conrad, D.; Courseau, J.; Muller, H.; Jaeger, R.; Kaps, C.; Klemm, D. O.; Kinne, R. W. Laser-structured bacterial nanocellulose hydrogels support ingrowth and differentiation of chondrocytes and show potential as cartilage implants. *Acta Biomater.* **2014**, *10* (3), 1341−53.
(36) Andrade, F. K.; Alexandre, N.; Amorim, I.; Gartner, F.; Maurício, A. C.; Luís, A. L.; Gama, M. Studies on the biocompatibility of bacterial cellulose. *J. Bioact. Compat. Polym.* **2013**, *28* (1), 97−112.
(37) Brown, R. M., Jr.; Willison, J. H.; Richardson, C. L. Cellulose biosynthesis in Acetobacter xylinum: visualization of the site of synthesis and direct measurement of the in vivo process. *Proc. Natl. Acad. Sci. U. S. A.* **1976**, *73* (12), 4565−9.
(38) Helenius, G.; Backdahl, H.; Bodin, A.; Nannmark, U.; Gatenholm, P.; Risberg, B. In vivo biocompatibility of bacterial cellulose. *J. Biomed. Mater. Res., Part A* **2006**, *76* (2), 431−438.
(39) Mello, L. R.; Feltrin, L. T.; Fontes Neto, P. T.; Ferraz, F. A. Duraplasty with biosynthetic cellulose: an experimental study. *J. Neurosurg.* **1997**, *86* (1), 143−50.
(40) Pertile, R. A.; Moreira, S.; Gil da Costa, R. M.; Correia, A.; Guardao, L.; Gartner, F.; Vilanova, M.; Gama, M. Bacterial cellulose: long-term biocompatibility studies. *J. Biomater. Sci., Polym. Ed.* **2012**, *23* (10), 1339−54.
(41) Czaja, W.; Krystynowicz, A.; Bielecki, S.; Brown, R. M., Jr. Microbial cellulose−the natural power to heal wounds. *Biomaterials* **2006**, *27* (2), 145−151.
(42) Czaja, W. K.; Young, D. J.; Kawecki, M.; Brown, R. M., Jr. The future prospects of microbial cellulose in biomedical applications. *Biomacromolecules* **2007**, *8* (1), 1−12.
(43) Axpe, E.; Oyen, M. L., Applications of Alginate-Based Bioinks in 3D Bioprinting. *Int. J. Mol. Sci.* **2016**, *17* (12), DOI: 10.3390/ijms17121976.
(44) Daly, A. C.; Critchley, S. E.; Rencsok, E. M.; Kelly, D. J., A comparison of different bioinks for 3D bioprinting of fibrocartilage and hyaline cartilage. *Biofabrication* **2016**, *8* (4), DOI: 10.1088/1758-5090/8/4/045002.
(45) Do, A. V.; Khorsand, B.; Geary, S. M.; Salem, A. K. 3D Printing of Scaffolds for Tissue Regeneration Applications. *Adv. Healthcare Mater.* **2015**, *4* (12), 1742−1762.
(46) Holzl, K.; Lin, S.; Tytgat, L.; Van Vlierberghe, S.; Gu, L.; Ovsianikov, A. Bioink properties before, during and after 3D bioprinting. *Biofabrication* **2016**, *8* (3), 032002.
(47) Ji, S.; Guvendiren, M. Recent Advances in Bioink Design for 3D Bioprinting of Tissues and Organs. *Front. Bioeng. Biotechnol.* **2017**, *5*, 23.
(48) Tsou, Y.; Khoneisser, P.; Huang, C.; Xu, X. Hydrogel as a bioactive material to regulate stem cell fate. *Bioactive Materials* **2016**, *1* (1), 39−55.
(49) He, Y.; Yang, F.; Zhao, H.; Gao, Q.; Xia, B.; Fu, J. Research on the printability of hydrogels in 3D bioprinting. *Sci. Rep.* **2016**, *6*, 29977.
(50) Jonoobi, M.; Oladi, R.; Davoudpour, Y.; Oksman, K.; Dufresne, A.; Hamzeh, Y.; Davoodi, R. Different preparation methods and properties of nanostructured cellulose from various natural resources and residues: a review. *Cellulose* **2015**, *22* (2), 935−969.
(51) Kawano, Y.; Kondo, T. Preparation of aqueous carbon material suspensions by Aqueous Counter Collision. *Chem. Lett.* **2014**, *43* (4), 483−485.
(52) Kondo, T.; Morita, M.; Hayakawa, K.; Onda, Y. Wet pulverizing of polysaccharides. Patent JP2005270891A, 2008.
(53) Kondo, T.; Kumon, D.; Mieno, A.; Tsujita, Y.; Kose, R. Preparation and characterization of two types of separate collagen nanofibers with different widths using aqeous counter collision as a gentle top-down process. *Mater. Res. Express* **2014**, *1* (4), 045016.
(54) Kondo, T.; Kose, R.; Naito, H.; Kasai, W. Aqueous counter collision using paired water jets as a novel means of preparing bio-nanofibers. *Carbohydr. Polym.* **2014**, *112*, 284−90.
(55) Kose, R.; Kasai, W.; Kondo, T. Switching surface properties of substrates by coating with a cellulose nanofiber having a high adsorbility. *Sen'i Gakkaishi* **2011**, *67* (7), 163−167.
(56) Kose, R.; Kondo, T. Size effects of cellulose nanofibers for enhancing the crystallization of poly(lactic acid). *J. Appl. Polym. Sci.* **2013**, *128* (2), 1200−1205.
(57) Kose, R.; Mitani, I.; Kasai, W.; Kondo, T. "Nanocellulose" as a single nanofiber prepared from pellicle secreted by Gluconacetobacter xylinus using aqueous counter collision. *Biomacromolecules* **2011**, *12* (3), 716−20.
(58) Tsuboi, K.; Yokota, S.; Kondo, T. Difference between bamboo- and wood-derived cellulose nanofibers prepared by the Aqueous Counter Collision method. *Nord. Pulp Pap. Res. J.* **2014**, *29* (1), 69−76.
(59) Atalla, R. H.; VanderHart, D. L. Native cellulose: A composite of two distinct crystalline forms. *Science* **1984**, *223* (4633), 283−285.
(60) Yamamoto, H.; Horii, F.; Hirai, A. In situ crystallization of bacterial cellulose II. Influences of different polymeric additives on the formation of celluloses Iα and Iβ at the early stage of incubation. *Cellulose* **1996**, *3* (4), 229−242.
(61) Matsuoka, M.; Tsuchida, T.; Matsushita, K.; Adachi, O.; Yoshinaga, F. A Synthetic Medium for Bacterial Cellulose Production by Acetobacter xylinum subsp. sucrofermentans. *Biosci., Biotechnol., Biochem.* **1996**, *60* (4), 575−579.
(62) Olderoy, M. O.; Lilledahl, M. B.; Beckwith, M. S.; Melvik, J. E.; Reinholt, F.; Sikorski, P.; Brinchmann, J. E. Biochemical and structural characterization of neocartilage formed by mesenchymal stem cells in alginate hydrogels. *PLoS One* **2014**, *9* (3), e91662.
(63) Yamamoto, H.; Horii, F. CPMAS carbon-13 NMR analysis of the crystals transformation induced for Valonia cellulose by annealing at high temperatures. *Macromolecules* **1993**, *26* (6), 1313−1317.

DOI: 10.1021/acsbiomaterials.9b00157
ACS Biomater. Sci. Eng. 2019, 5, 2482−2490

(64) Yi, H. G.; Choi, Y. J.; Jung, J. W.; Jang, J.; Song, T. H.; Chae, S.; Ahn, M.; Choi, T. H.; Rhie, J. W.; Cho, D. W. Three-dimensional printing of a patient-specific engineered nasal cartilage for augmentative rhinoplasty. *J. Tissue Eng.* **2019**, *10*, 204173141882479.
(65) Halib, N.; Perrone, F.; Cemazar, M.; Dapas, B.; Farra, R.; Abrami, M.; Chiarappa, G.; Forte, G.; Zanconati, F.; Pozzato, G.; Murena, L.; Fiotti, N.; Lapasin, R.; Cansolino, L.; Grassi, G.; Grassi, M., Potential Applications of Nanocellulose-Containing Materials in the Biomedical Field. *Materials (Basel)* **2017**, *10* (8), DOI: 10.3390/ma10080977.
(66) Jorfi, M.; Foster, E. J. Recent advances in nanocellulose for biomedical applications. *J. Appl. Polym. Sci.* **2015**, *132* (14), 41719.

DOI: 10.1021/acsbiomaterials.9b00157
ACS Biomater. Sci. Eng. 2019, 5, 2482−2490